Supplementary Information

sp^3-Linked Dimeric Carbazole-Based p-Type Hosts for Exciplex-Driven Green TADF OLEDs

Shinyoung Kim, Ha Yeon Kim, Subin Kwon, Yeseo Lee, Simhyeon Lee, Chang Seop Hong, Sungnam Park, Min Ju Cho*, Dong Hoon Choi*

Department of Chemistry, Center for Advanced Molecular Science, Korea University,
145 Anam-ro, Seongbuk-gu, Seoul 02841, Korea

*Corresponding authors: M. J. Cho (E-mail: chominju@korea.ac.kr); D. H. Choi (E-mail: dhchoi8803@korea.ac.kr)

1. General Information

1.1. Instrument

The chemical structures of the synthesized compounds were analyzed using ^{1}H and ^{13}C NMR spectroscopy in deuterated chloroform (Cambridge Isotope Laboratories) with a Varian Mercury 500 MHz spectrometer. Matrix-assisted laser desorption ionization time-of-flight mass spectrometry (MALDI-TOF/TOF™ 5800 system (AB SCIEX)) was used to confirm the mass of each compound. The experiments were conducted at the Korea Basic Science Institute (Seoul, Korea).

The absorption spectra of the materials in toluene and the neat films were acquired using an Agilent 8453 UV-Vis spectrophotometer. Fluorescence spectra at 77 K and 298 K, and phosphorescence spectra at 77 K with a delay time of 1.0 ms, were recorded using an F-7100 fluorescence spectrophotometer by HITACHI. The absolute photoluminescence quantum yields of the films were determined with an FP-8500 spectrofluorometer from JASCO, which was equipped with an integrating sphere (ILF-835). In the TRPL measurements, film samples

were placed in a cryostat (Janis, VPF-100) under high vacuum (≤ ~10^{-2} mTorr) and excited by 355 nm laser pulses generated via third-harmonic conversion of a 1064 nm Nd:YAG laser (Q-smart 850, Lumibird FR). The emission signals were collected using a photomultiplier tube (Hamamatsu R955) coupled to a 100 MHz digital oscilloscope (Keysight DSO-X 3014A).

The film roughness and thickness were assessed using atomic force microscopy (AFM) in noncontact mode with a Park Systems XE-100 instrument.

Differential scanning calorimetry (Mettler STARe) was used to analyze the thermal characteristics of the emitters, such as glass transition (T_g), crystallization (T_c), and melting (T_m) temperatures, in an N_2 atmosphere. Thermogravimetric analysis (Mettler STARe) was conducted at a heating rate of 10 °C min^{-1} under N_2 to ascertain the decomposition temperature (T_d) of each compound.

The electrochemical properties (oxidation and reduction potentials) of the hosts in solution and the films were analyzed through cyclic voltammetry at a scan rate of 50 mV/s using a potentiostat (VSP-3e). Thin films of the three hosts were fabricated on Pt plates employing a drop-casting technique. Ag/AgCl and a platinum wire (diameter: 0.5 mm) served as the reference and counter electrodes, respectively. Tetrabutylammonium hexafluorophosphate (Bu_4NPF_6, 0.10 M) in distilled acetonitrile was utilized as the electrolyte. Grazing-Incidence Wide-Angle X-ray Diffraction(GIWAXD) was performed on polymer thin films deposited on SiO2 wafers using the 9A beamline at the Pohang Accelerator Laboratory (energy =11.56 keV, pixel size = 0.0781 mm, λ = 1.07 Å, 2θ = 14.820°).

1.2. Angle-dependent PL experiments

The z-direction was perpendicular to the glass substrate, and the x- and y-directions were parallel to the glass substrate. The orientation factor, Θ, is defined as follows, where p_j is the transition dipole oriented in j-direction.

$$\Theta = \frac{[p_z]}{[p_x] + [p_y] + [p_z]}.$$

Θ was 0.33 when the orientation of the dopants was isotropic (or randomly oriented), and Θ = 0 when the dopant orientation was horizontal. The power radiated from the transition dipoles oriented in the x-, y-, and z-directions are expressed as $P^{\parallel,TM}$, $P^{\parallel,TE}$, and $P^{\perp,TM}$, respectively. The symbols $\parallel$ and $\perp$ indicate the orientations of the transition dipoles (i.e., parallel (horizontal) and perpendicular (vertical) to the substrate plane, respectively). Additionally, TM and TE represent the polarization of the emitted light (i.e., p-polarized (transverse magnetic, TM) and s-polarized light (transverse electric, TE)). The total radiated power from the dipole without any interfaces was described by taking the dipole distribution as follows:

$$P_0 = \Theta \cdot P_0^{\perp} + (1 - \Theta) P_0^{\parallel},$$

where $P_0^{\perp}$ and $P_0^{\parallel}$ represent the power radiated from the vertical- and horizontal-oriented dipoles, respectively.

$$P_0^{\perp} = \frac{\mu_0^2 \omega^4}{12\pi\varepsilon_0 c^3} n_z,$$

$$P_0^{\parallel} = \frac{\mu_0^2 \omega^4}{12\pi\varepsilon_0 c^3} \cdot n_x \cdot \frac{3n_x^2 + n_z^2}{4n_x^2},$$

where μ_0 is the dipole moment, ω is the oscillation frequency, and c is the speed of light. However, if the emitting layer (EML) was sandwiched between two layers, as shown in Fig. S10, the Purcell effect in dielectric media should be considered. The Purcell factor can be expressed based on Kuhn's model.

$$F = \frac{P^{\perp,\parallel}}{P_0} = 1 + \frac{3qn^2}{2\mu_0 k^3} Im(E_0) = \int_0^{\infty} K^{\perp,\parallel}(u) du,$$

where F is the Purcell factor, k is the wavenumber, u is the normalized in-plane wave vector, E_0 is the reflected electric field at the dipole position, and $K^{\perp,\parallel}$ represents the power dissipation function.

Additionally, the embedded locations of the emitters in the EML should be considered in theoretical calculations. As shown in Fig. S10, the emitters are located at distances of s and d from each interface. Furthermore, the EML was sandwiched between air and glass substrate layers. In this case, the power dissipation functions can be obtained by calculating the radiated electric field from the emitter, using the appropriate boundary conditions. Accordingly, the power dissipation functions depend on the refractive indices (n_z, n_x, n_2, and n_3) of the three layers, the Fresnel's reflection coefficients at the interfaces, the distances of the emitter from the interfaces (i.e., s and d), and the EML thickness (i.e., $s + d$), as shown in Fig. S10. The radiated power spectrum was described as a function of the detection angle, θ, and wavelength, λ, as follows:

$$I(\theta,\lambda) = \left[\Theta \cdot P_0^{\perp} \cdot K'^{\perp,TM}_{out}(\theta,\lambda) + (1-\Theta) \cdot P_0^{\parallel} \cdot \left\{K'^{\parallel,TM}_{out}(\theta,\lambda) + K'^{\perp,TE}_{out}(\theta,\lambda)\right\}\right] \cdot S_{PL}(\lambda),$$

where $S_{PL}(\lambda)$ is a wavelength-dependent radiative property, the PL spectral density. All the parameters, including the refractive indices and EML thickness, were experimentally and theoretically obtained. Therefore, the radiated power spectrum, $I_n(\theta,\lambda)$, can be readily simulated as a function of the Θ.

However, when the emitters were randomly doped in the EML, the position of each emitter along the z-direction was considered in the radiated power spectrum because the position of the emitter (i.e., s and d) affects the equation of the radiated power spectrum. In this case, the assumption that the EML is divided into N layers along the z-axis and the emitters are placed at the interfaces between the layers is adopted to consider the randomly doped emitters in the EML. The value of N can be chosen based on the thickness of the EML (s + d). With this

assumption, the total radiated power spectrum from the EML, resulting from all interfaces between the layers (N − 1), can be described by the sum of the radiated power spectra as follows:

$$I_{total}(\theta,\lambda) = \sum_{n=1}^{N-1} I_n(\theta,\lambda),$$

where $I_n(\theta,\lambda)$ is the power spectrum radiated from the interface between the nth and (n+1)th layers. In this equation, s_n and d_n are the vertical positions of the dopant molecules in the EML with a thickness of l (i.e., $d_n = l \times \left(\frac{n}{N}\right)$ and $S_n = 1 - d_n$).

Fig. S1. (a) The orientation of the transition dipoles. (b) schematic illustration of the angle-dependent PL measurement with thin films on a glass substrate.

Angle-dependent PL measurements were performed on the doped samples prepared by solution casting on a quartz substrate. Thereafter, the film samples were placed on a fused silica half-cylinder. An index-matching gel (G608N3. Thorlabs, Inc.) was inserted between the glass substrate and half-cylinder to remove the air and match the refractive index. The film sample on the fused silica half-cylinder was excited with laser pulses generated by an Nd:YAG laser (355 nm). The p-polarized light with an incident angle of 45° was directed to the film sample. The photoluminescent emission from the sample was transmitted through a half-cylinder placed below the glass substrate and collected at a series of angles using an optical fiber, mounted on a motorized rotational stage, and coupled with a monochromator and charge-coupled device (CCD). To selectively obtain only the p-polarized emissions, a polarizer was placed in front of the optical fiber. The angle was automatically controlled by a motorized rotational stage (URS100BPP, Newport Corporation) from 0° to 90°, with a resolution of 1°. The thickness of the host dopant film on the glass substrate was 35 nm. Matlab codes were used to determine the molecular orientation in the thin films with the fitting parameter of Θ.

1.3. OLED Device Fabrication

OLED devices were produced on glass substrates covered with a transparent ITO layer (150 nm, with a sheet resistance of 15 Ω cm^{-2} and an active pattern size of 2 × 2 mm) as the anode. The substrates underwent a cleaning process in distilled water for 10 min and isopropanol for 20 min using an ultrasonic bath, followed by drying with hot air. PEDOT:PSS was directly spin-coated onto an ITO plate to create a hole injection layer (30 nm) and then heated at 155 °C for 15 min on a hot plate. A mixture of a host (CzCzPh:SiTrzCz2, FL-PP:SiTrzCz2, Si-PP:SiTrzCz2) and t4CzIPN emitter (96:4 w/w, 0.5 wt% in toluene) was spin-coated to form the emitting layer. The thickness of the EML was measured using a spectroscopic ellipsometer

(Woollam Alpha-SE). BmPyPB (50 nm) served as the electron-transporting layer, and LiF (1 nm) and Al (100 nm) were vacuum-deposited in an inert chamber at 5×10^{-6} Torr. The fabricated device consisted of ITO (150 nm) and PEDOT:PSS (30 nm), hosts: emitter (30 nm), BmPyPB (50 nm), LiF (1 nm), and Al (100 nm). The fabrication process was conducted under ambient conditions before transferring the substrates to a thermal vacuum evaporator for the evaporation of BmPyPB, LiF, and Al.

1.4. Single Carrier Devices

To compare the charge carrier transport abilities of host-containing HODs and EODs, they were fabricated on patterned ITO-coated glass with a sheet resistance of 15 Ω cm^{-2} (AMG Corp.). The HOD configurations consisted of ITO (150 nm), PEDOT:PSS (30 nm), host (30 nm), TAPC (10 nm), and Al (100 nm). The EOD configurations included ITO (150 nm), Al (40 nm), host (30 nm), BmPyPB (50 nm), LiF (1 nm), and Al (100 nm). PEDOT:PSS was deposited as received and annealed at 155°C for 15 minutes. The hosts were then spin-coated as required. BmPyPB, LiF, and Al were subsequently deposited using a thermal evaporator.

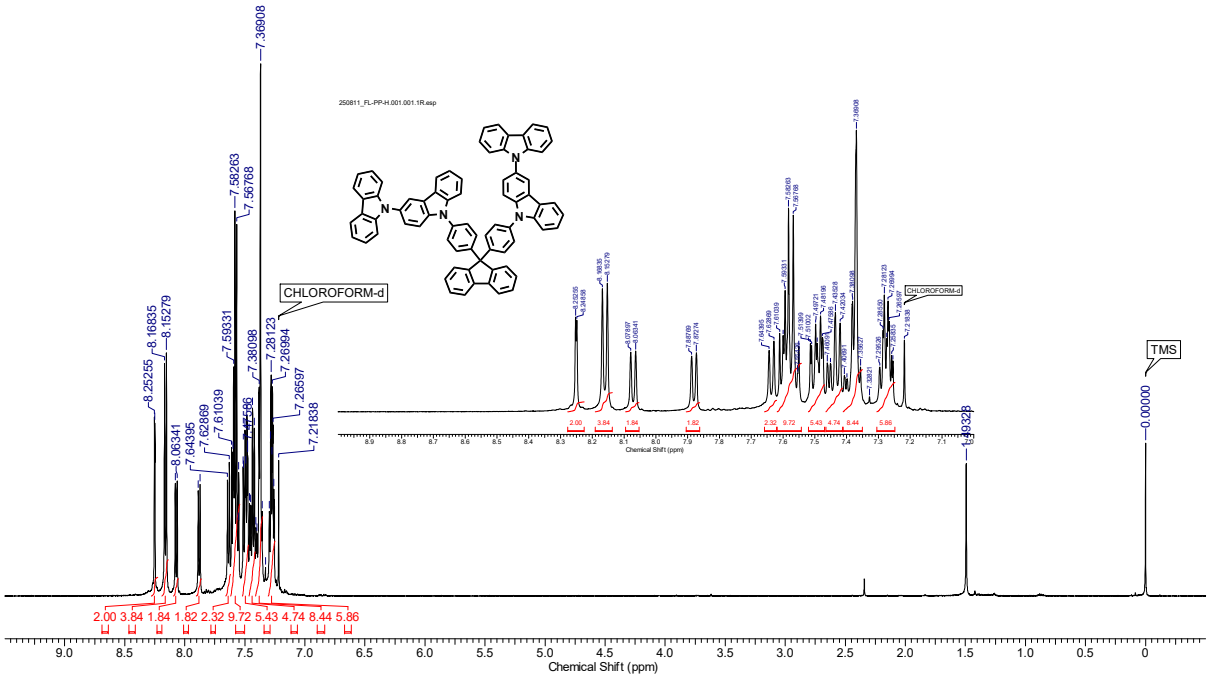

Fig. S2. ^{1}H NMR spectrum of FL-PP (**3**)

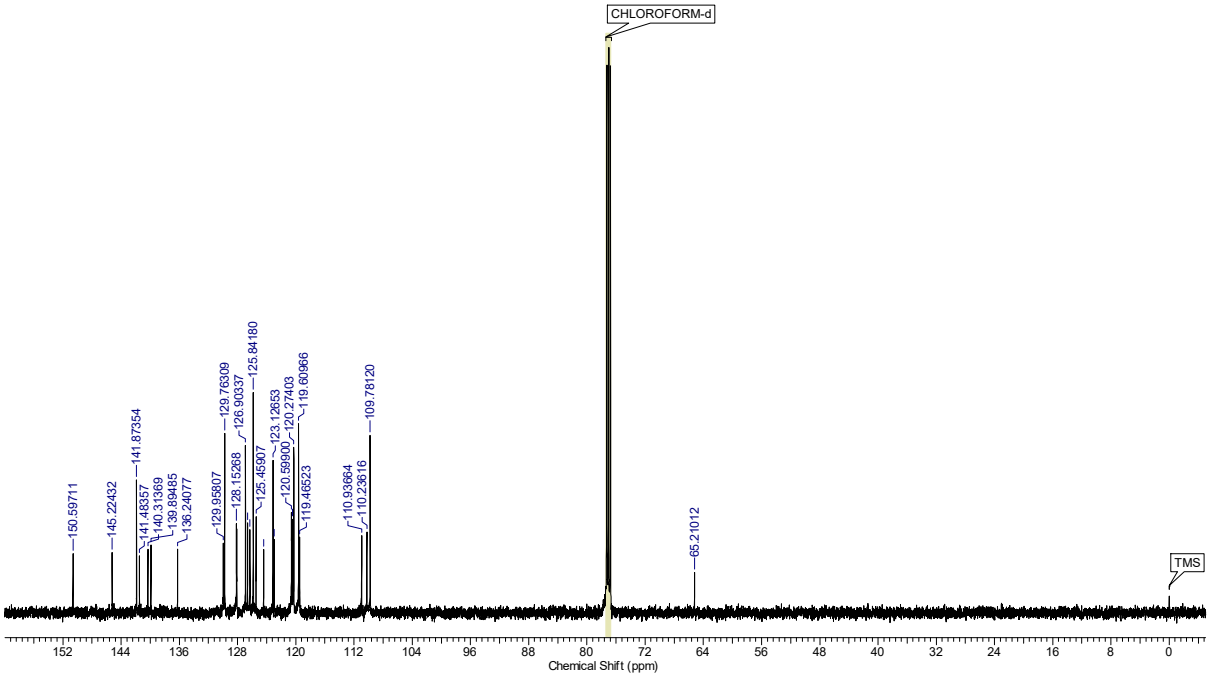

Fig. S3. ^{13}C NMR spectrum of FL-PP (**3**)

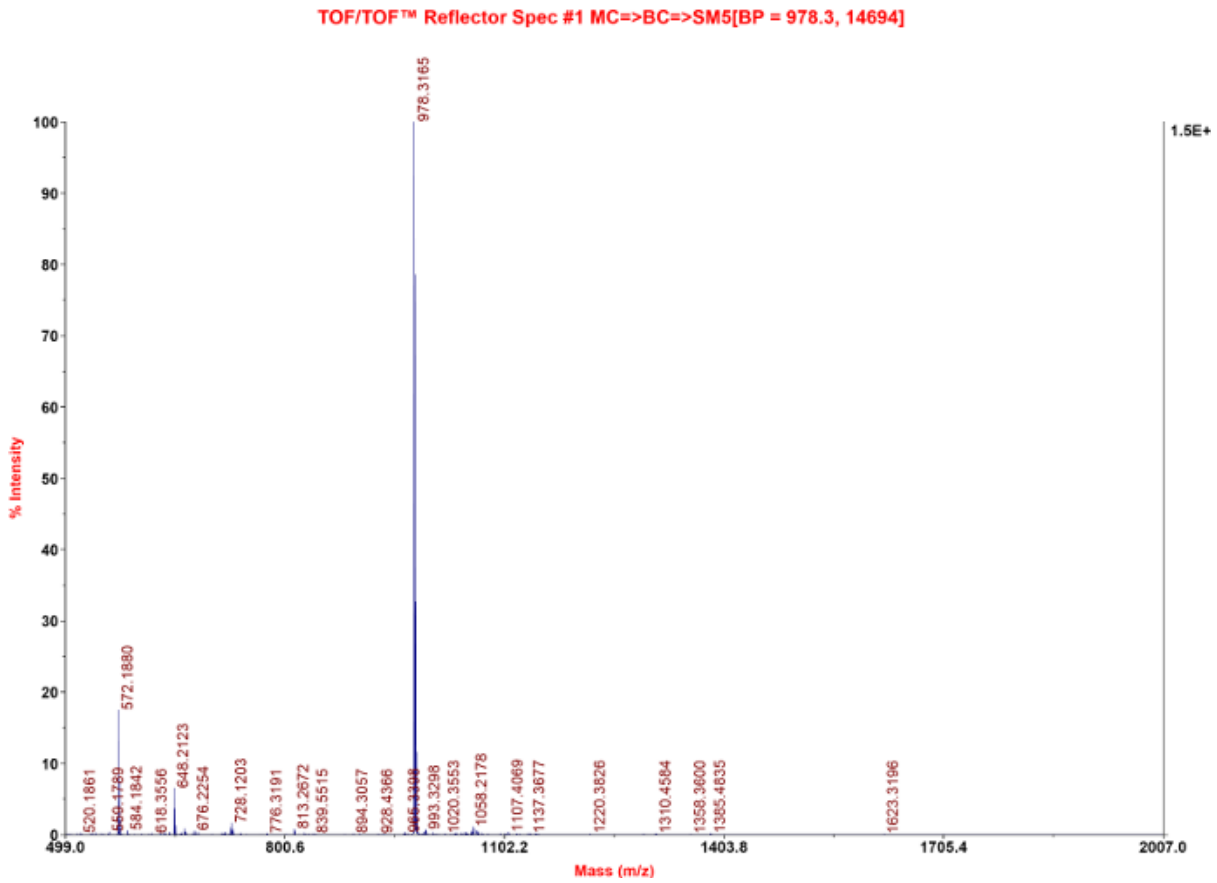

Fig. S4. MALDI-TOF mass spectrum of FL-PP (**3**)

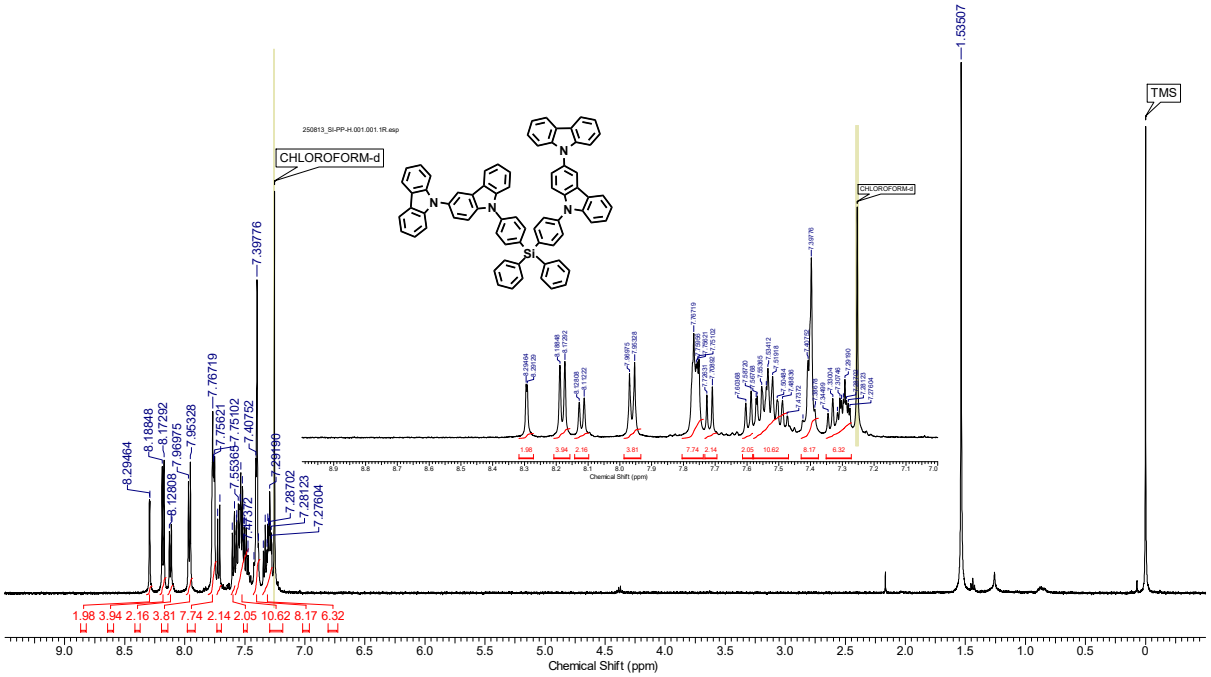

Fig. S5. ^{1}H NMR spectrum of Si-PP (**5**)

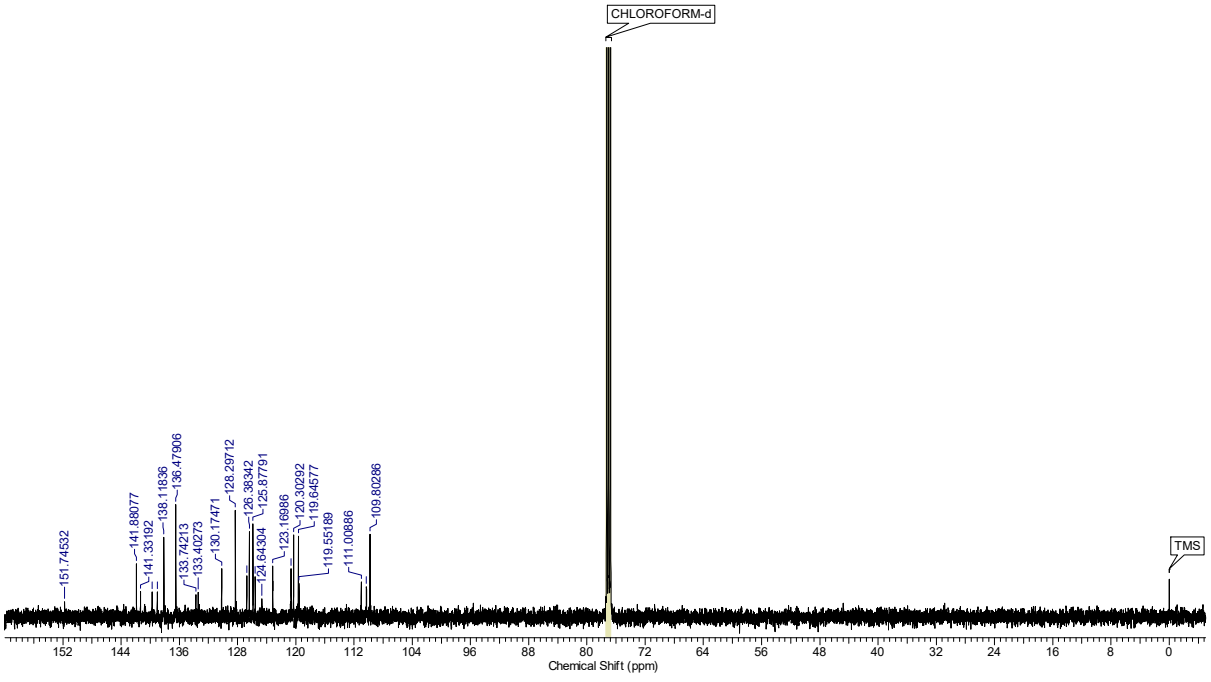

Fig. S6. ^{13}C NMR spectrum of Si-PP (**5**)

Fig. S7. MALDI-TOF mass spectrum of Si-PP (**5**)

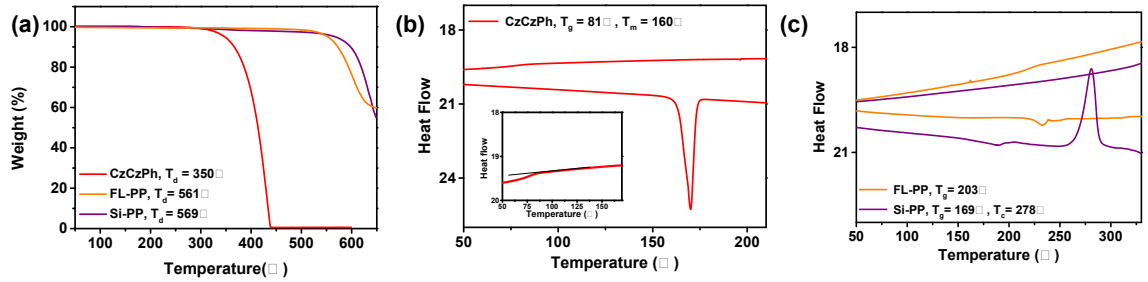

Fig. S8. TGA and DSC thermograms of CzCzPh, FL-PP and Si-PP. (temperature rate 5 °C, N_2 atmosphere)

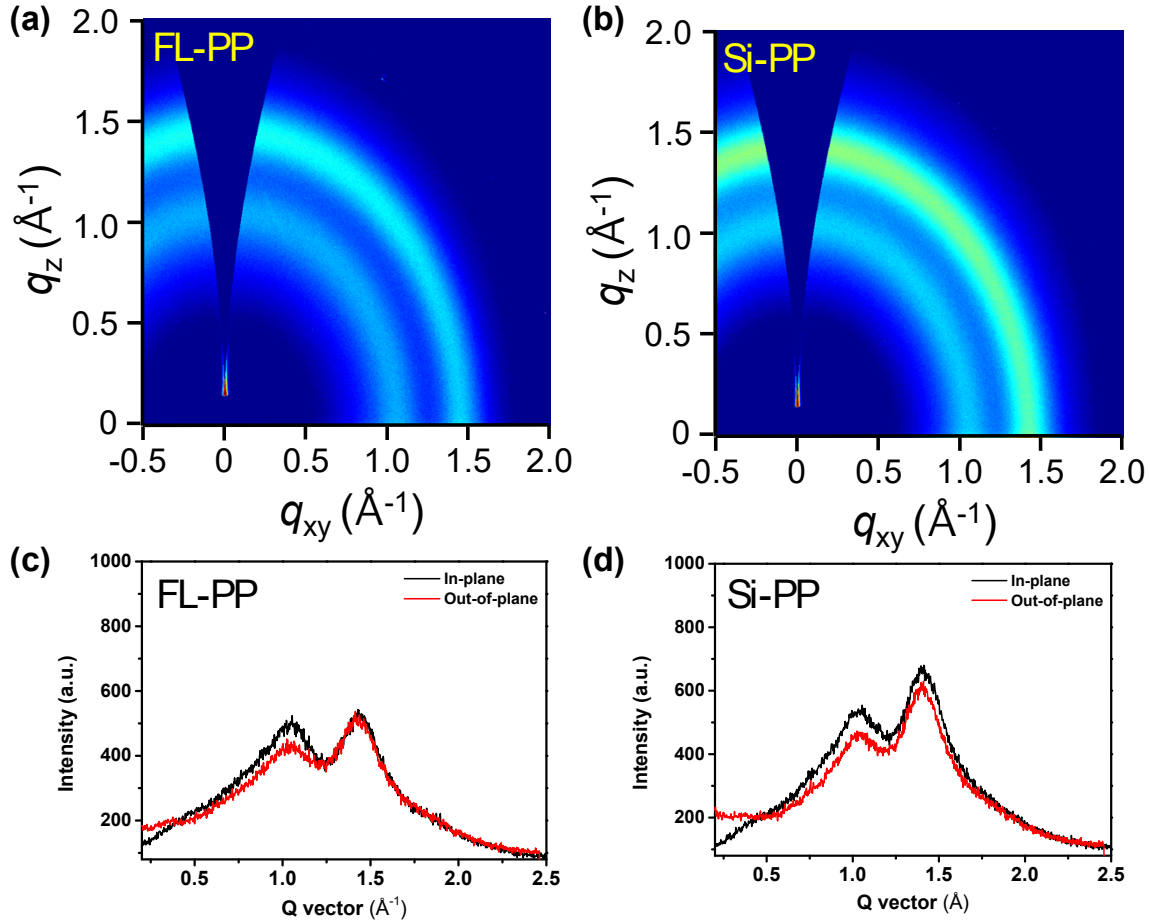

Fig. S9. Grazing-incidence wide-angle X-ray diffraction (GIWAXD) patterns of (a) FL-PP and (b) Si-PP thin films. The corresponding one-dimensional line-cut profiles are shown below each 2D pattern.

To further probe the structural origin of the different film morphologies, grazing-incidence wide-angle X-ray diffraction (GIWAXD) measurements were performed (Fig. S9). The FL-PP film shows predominantly diffuse scattering with broad amorphous halos, whereas the Si-PP film exhibits weak and broadened diffraction features superimposed on the amorphous halo, indicating the presence of limited or nanoscale molecular ordering. These results are consistent with the DSC analysis and suggest that the diphenylsilane core in Si-PP promotes partial ordering, while the cardo-type fluorene core in FL-PP stabilizes an amorphous morphology.

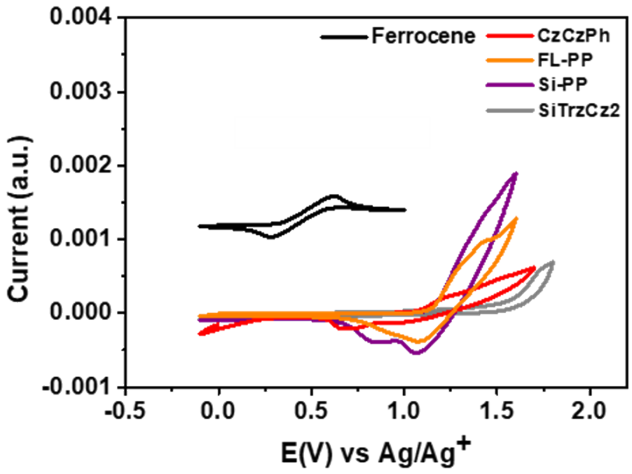

Fig. S10. Cyclic voltammograms of CzCzPh, FL-PP, Si-PP, and SiTrzCz2 in film states.

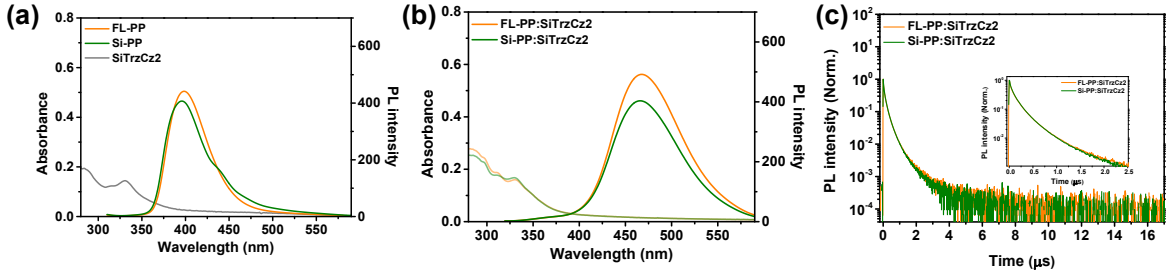

Fig. S11. (a) UV–vis absorption spectrum of SiTrzCz2 and PL spectra of FL-PP and Si-PP in the film state. (b) UV–vis absorption and PL spectra of blend films composed of donor materials and SiTrzCz2 acceptor in the film state. (c) Time-resolved photoluminescence decay profiles of the two blend films.

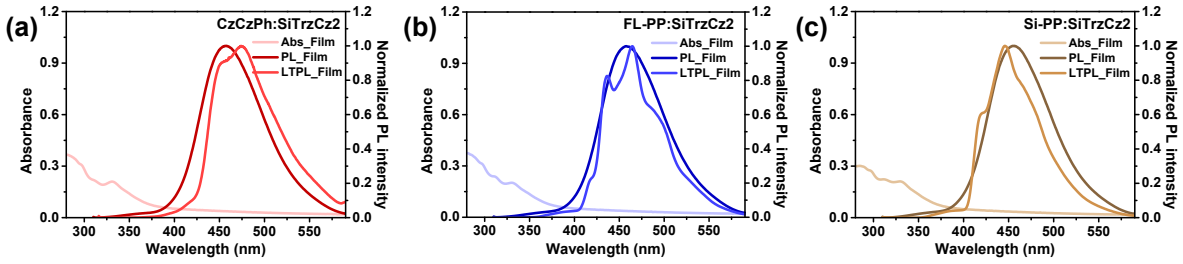

Fig. S12. UV-vis absorption, fluorescence (measured at 298 K), and phosphorescence spectra (measured at 77K) of (a) CzCzPh:SiTrzCz2, (b) FL-PP:SiTrzCz2, and (c) Si-PP:SiTrzCz2 in the film state.

Table S1. Photophysical and electrochemical properties of blend film with three p-type hosts and the n-type host SiTrzCz2, including absorption and emission wavelengths, singlet and triplet energies, ΔE_{ST}.

Compound	Absorption (nm)	PL (nm)	E_S/E_T (eV)	ΔE_{ST} (eV)	E_g (eV)
CzCzPh:SiTrzCz2	297, 310, 332	457	3.16/3.07	0.09	3.35
FL-PP:SiTrzCz2	297, 310, 331	458	3.16/3.06	0.10	3.35
Si-PP:SiTrzCz2	297, 311, 329	456	3.18/3.07	0.11	3.34

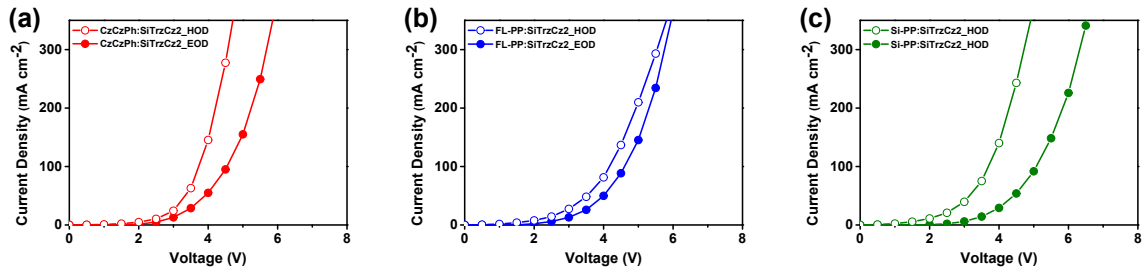

Fig. S13. Current density–voltage (J–V) characteristics of (a) CzCzPh:SiTrzCz2, (b) FL-PP:SiTrzCz2, and (c) Si-PP:SiTrzCz2 for hole-only devices and electron-only devices.

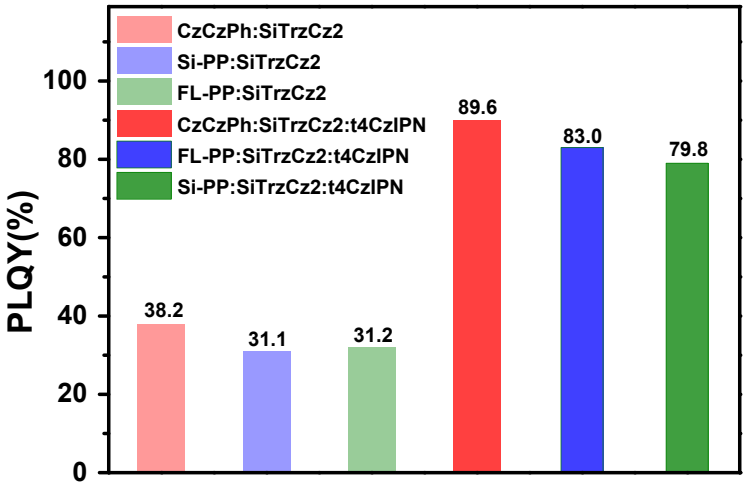

Fig. S14. PLQY of neat and 4 wt% t4CzIPN-doped films of CzCzPh:SiTrzCz2, FL-PP:SiTrzCz2, and Si-PP:SiTrzCz2, measured at an excitation wavelength of 300 nm.

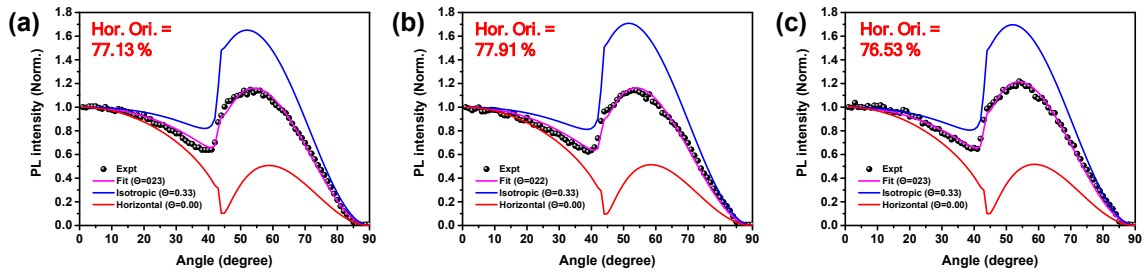

Fig. S15. Angle-dependent photoluminescence (PL) of (a) CzCzPh:SiTrzCz2:t4CzIPN(Device 1), (b) FL-PP:SiTrzCz2:t4CzIPN(Device 2), and (c) Si-PP:SiTrzCz2:t4CzIPN (Device 3) films measured on quartz substrates. Experimental data (symbols) are fitted with optical models assuming different dipole orientations.

Fig. S16. (a) Schematic of the OLED device configuration with energy level alignment. (b) Current density–voltage–luminance (J–V–L) characteristics, including (c) luminance–external quantum efficiency curves, (d) luminance–power efficiency–current efficiency curves, and (e) electroluminescence spectra, of devices employing an exciplex host doped with t4CzIPN. The EML was annealed at 130 °C for 30 min.

Table S2. Comparison of representative mCP:PO-T2T exciplex strategies and the present work.

Item	Materials Today 2024, 74, 109–120	Chem. Eng. J. 2023, 461, 141921	This work (solution-processed exciplex host)
Exciplex platform	mCP/PO-T2T interfacial exciplex	mCP/PO-T2T interfacial exciplex	FL-PP or Si-PP (p-type) + SiTrzCz2 (n-type) bulk-blend exciplex host
Core innovation	Device architecture (multi-interfacial exciplex + ultrathin emitting layer)	Device architecture (interfacial exciplex sensitization + ultrathin emitting layer)	Molecular design of p-type host (sp^3-linked dimerization) for solution processing & thermal robustness
Typical emitter strategy	Doping-free or ultrathin phosphorescent emitting layer (Ph-UEML) sensitized by exciplex	Ultrathin emitting layer sensitized by exciplex	Conventional doped EML (e.g., t4CzIPN doped into exciplex host blend)
Processing	Thickness-controlled architectures (vacuum process))	Thickness-controlled architectures (vacuum process)	Solution-processed EML (spin-coating) with high-temperature drying/annealing tolerance
Key distinguishing mechanism	Efficiency from engineered interfaces + ultrathin emissive layers	Efficiency from interfacial exciplex sensitization	Efficiency + stability from amorphous stabilization of p-host via sp^3 dimerization (structure–morphology–device linkage)
Representative performance (as reported)	High EQE in monochrome/white devices	High EQE in monochrome/white devices	Green TADF-OLED EQE > 20% and strong retention after annealing (FL-PP system)